The CSI Journal on
Computer Science and Engineering
Vol. 20, No. 1, 2026
Pages 9-26
doi.org/10.22034/jcse.2025.537565.1057
Regular Paper

Performance Improvement of CIGS Thin-Film Solar Cells by Incorporating an ITO Photoanode and Designing a Structured Back Layer

Reza Kiani, Majid Fouladiyan*, Seyyed Mohammad Jalal Rastgar Fatemi
Faculty of Electrical Engineering-Saveh Branch, Islamic Azad University, Saveh, Iran
Email: Majid.fouladian@iau.ac.ir

Abstract

Copper Indium Gallium Selenide (CIGS) thin-film solar cells are well known for their intrinsic stability and suitable direct bandgap, making them promising candidates for high-efficiency photovoltaic applications. This study aims to improve the performance of CIGS solar cells by incorporating pitch-like gaps in the back contact layer to reduce minority carrier recombination. Using Silvaco TCAD simulations, the effects of various gap widths and material properties on cell efficiency were analyzed. Results indicated that an optimal gap width of 200 nm, combined with increased doping concentration and charge density in the absorber layer above 1 cm^{-3}, significantly boosted performance. Additionally, tuning the doping profiles of other layers mitigated the adverse effects of the back layer's high resistivity and low conductivity. Furthermore, integrating a transparent ITO photoanode improved front-side light transmission. Collectively, these design modifications increased the device efficiency from 20.8% to 27.5%, demonstrating a substantial improvement in both optical and electrical characteristics of the CIGS solar cell architecture.

Keywords: CIGS solar cells, minority carrier recombination, back layer engineering, Silvaco simulation, ITO photoanode.

1. Introduction

Air pollutants emitted from hydrocarbon sources, exacerbated by climate change and events like floods, droughts, water shortages, and wildfires, as well as incurable diseases such as cancer, respiratory illnesses, and blood and skin disorders [1–3], have prompted scientists to explore alternative energy sources. This has led to a shift away from fossil fuels like coal, oil, gas, and hydrocarbon derivatives towards cleaner options such as nuclear, hydroelectric, wind, wave, and geothermal power. Solar energy is one of the available and constant energy sources that radiates to the Earth with varying intensities, heating different regions, and can be harnessed by humans. Fortunately, with advancements in science and technology, it is now possible to convert solar energy into electricity using solar technology.

Solar cells are divided into several categories based on their structural type and efficiency, one of the best known is CIGS thin film solar cells with an absorption layer called chalcopyrite as shown in Figure 1. To increase their efficiency, materials containing copper, indium, gallium, and selenide compounds of different densities are used, which effectively absorb or transmit the light.

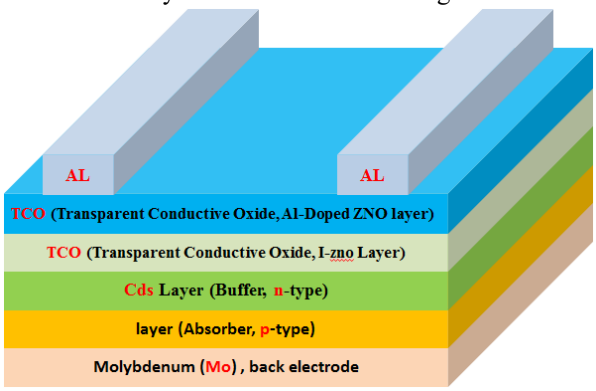

Figure 1. The general structure of a CIGS thin film solar cell [1].

$CuIn_{(1-x)}Ga_{(x)}Se_2$ chalcopyrite solar cells have a direct bandgap, and researchers have reported their efficiency. For example, a solar cell with an efficiency of 20.4% using a low-temperature process with a polyimide substrate [1], and an efficiency of 22.6% using a high-temperature process with glass [2], have been reported. The main problem with light absorption in solar cells is the reflection of light when it strikes the cell surface, resulting in approximately 4% of the incoming light being reflected [3]. It should be noted that CIGS solar cells are cheaper to produce than crystalline silicon [4,5] and can be used in buildings, clothing, and space equipment because they are more flexible and lighter [6] and are resistant to radiation and environmental conditions [7]. One of the most effective ways to prevent light reflection is to use anti-reflective layers in low refractive index materials such as (MgF_2, Al_2O_3, and SiO_2) compared to high refractive index materials such as (ZnS, TiO_2, and CeO_2) [8] . Research shows that in 2020, the efficiency of CIGS solar cells reached 20.52% using an anti-reflective magnesium fluoride layer (MgF_2) with a thickness of 0.11 µm [9] (Figure 2).

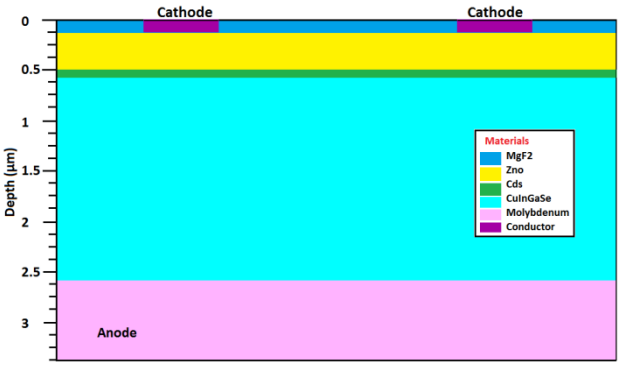

Figure 2. Effect of MgF2 anti-reflective layer on CIGS solar cells [9].

According to the mentioned contents, important results can be deduced:

1. The use of an MgF_2 anti-reflective layer improves the short-circuit current density and energy conversion efficiency (the thickness of the reflective layer should not be more than a quarter of the wavelength of the incident light, because with greater thicknesses the light reflection increases and the cell efficiency decreases).

2. Increasing the thickness of the CdS buffer layer reduces the number of photons transferring energy to the absorbing layer and the absorption of light in the absorbing layer decreases. Therefore, to reduce light absorption losses, it is necessary to minimize the thickness of the buffer layer.

3. Increasing the thickness of the ZnO window layer increases the generation of electron-hole pairs, which leads to a decrease in efficiency.

4. Increasing the thickness of the CIGS absorption layer, the VCO and ISC parameters also increase and improve the efficiency. In fact, the generation of electron-hole pairs is greater at shorter wavelengths and causes an increase in VCO and ISC.

5. Reducing the CIGS thickness causes a recombination process at the back junction and as a result VCO and ISC decrease. In general, by increasing the thickness of the CIGS layer, the efficiency increases continuously and non-linearly.

In another research in the field of ultra-thin Cu (In, Ga) Se_2 solar cells with high efficiency, by creating a pitch (2 µm cell gap and 0.2 µm cell width with a density of 10^{16} cm^{-3}) on the silver substrate an efficiency value of 23.35% has been achieved (the lattice constant of silver Ag is close to both the Al_2O_3 layer and the CIGS absorption layer) [10]. It is shown in Figure 3.

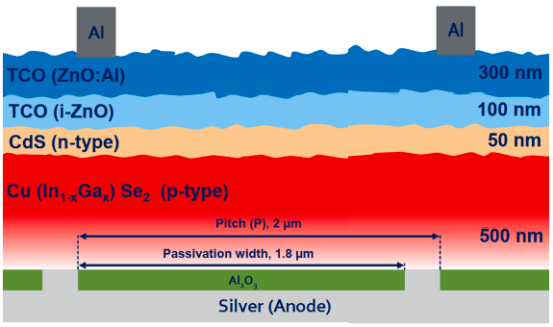

Figure 3. Effect of pitch on increasing the efficiency of CIGS solar cell [10].

The aforementioned paper investigated the effect of cell spacing, aperture width, absorption layer thickness, doping, and Ga=Ga/(Ga+In) ratio on the performance of CIGS thin film solar cells. Therefore, the following results are obtained:

1. A thin layer of Al_2O_3 with a high negative charge density makes the back layer passive and reduces recombination losses in it.

2. Deactivation of the back layer is effective in the CIGS absorbing layer.

3. Al_2O_3 back passive layer with high positive charge density and high contact resistance with the Ag/CIGS layer causes weak passivation.

4. The width and distribution of the back layer are limited.

5. The cathode terminal should have a higher function than the back layer.

6. The creation of pitch balances the work function of the anode and cathode (the work function has a ramp mode to allow the electrons to move).

Another study in 2020 on CIGS thin-film solar cells used a 120-nm thick magnesium fluoride (MgF2) layer as an anti-reflective coating (ARC) to reduce light reflection from the front surface, thereby increasing the amount of light entering the cell. Accordingly, the thickness of each designed layer is shown in Figure 4 [11].

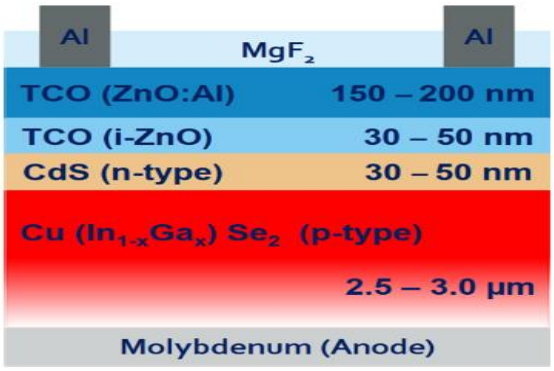

Figure 4. Light penetration into a CIGS cell with an MgF_2 thickness of 120 nm [11].

In another study aimed at reducing parasitic absorption, research was conducted to improve the performance of CIGS solar cells, and it was concluded that decreasing the thickness of the CdS buffer layer increases the optical current. However, two parameters—open-circuit voltage (VOC) and fill factor (FF)—were found to decrease [12]. In this study, the CdS buffer layer is considered to be less than 30 nm. Because of its small band gap, CdS tends to absorb significant interference in the blue wavelength range. To solve this defect, indium tin oxide (ITO) with a larger bandgap has been used as a buffer layer as an alternative. This replacement increased productivity and efficiency without negatively affecting V_{OC} and FF.

ITO is an environmentally friendly material with a thin thickness and band gap (3.5-4.3 eV), which helps to increase the short-circuit current (Jsc), which increases the efficiency of the CIGS solar cell by about 6% Compared to a conventional cell. In addition, they used ZnMgO (ZMO) material, which has a higher transparency and a higher bandgap, instead of the usual ZnO window layer, which increased the short-circuit current Jsc (The direct optical band gap of ZMO is 2.1 eV. The edges of the conduction band 4.2 eV and the capacitance band 6.3 eV are below the vacuum level) [13].

In a study where conventional CdS buffer layers were replaced by a double buffer layer of Zn (O, S, $OH)_x$ /$Zn_{0.8}$ $Mg_{0.2}O$, V_{OC} increased by about 15 mV. The fill factor and short-circuit current also improved, and the device efficiency increased almost 0.5% compared to cells with CdS buffer. In fact, the double buffer layer extended the lifetime of the minority carrier (τ) and reduced the carrier recombination process, and this resulted in the increased efficiency of 23.35% [14]. The increase in Ga density in CIGS with a conventional cds buffer layer (1.15 eV bandgap) is limited and leads to reduced efficiency. However, if we examine the layer $Cd_{(1-y)}Zn_{(y)}S$ instead of Cds and add another layer called void layer (OVC) with Ga and Zn contents of 0.7 and 0.6, respectively, the efficiency increases to about 23.71% (Figure 5) [15].

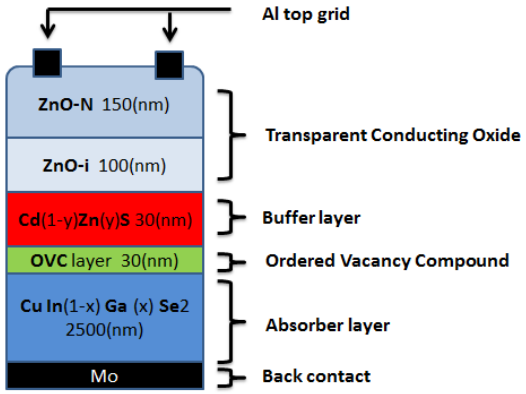

Figure 5. Use of $cd_{(1-y)}Zn_{(y)}$ S layer instead of cds [15].

To improve the efficiency of CIGS, the magnesium fluoride layer (MgF_2) is utilized as an anti-reflective coating to maximize the optical flow caused by the incident light intensity and the effect of the minority carrier lifetime and improve the efficiency to 24.5% [16]. Some studies used ZMO instead of ZNO and ITO instead of Cds and achieved a 7.5% improvement over conventional solar cells according to Figure 6 [17].

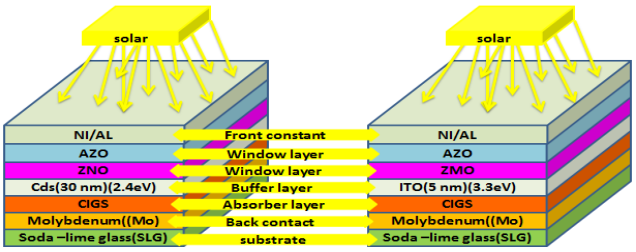

Figure 6. Replacement of ZNO and Cds layers with ZMO and ITO layers[17].

Reasons for not using CdS include the minimization of optical losses in the short-wavelength range [16], the toxicity of cadmium sulfide, and the limitations of its deposition method [17]. The most suitable coating technique for ITO thin films at low temperatures is the atomic layer deposition (ALD) method [18,19]. Buffer layer with donor-donor doping plays an important role in improving the overall efficiency of the solar cell, and with a higher electron carrier density, it expands the CIGS-depleted region and improves the efficiency [20,21]. The formation of correct bond alignment at the common boundary of different layers has a significant effect on reducing surface recombination and improving productivity [22].

At the end of this introduction, a summary of the reviewed studies is presented. Previous research has explored various methods to improve the efficiency of CIGS solar cells, particularly by addressing challenges such as high carrier recombination rates and low conductivity. Although progress has been made, the efficiency of CIGS cells still faces limitations. This study aims to tackle these issues by applying a dual optimization approach: enhancing the transparency of the front electrode using an ITO layer and reducing recombination at the back layer with a pitch structure. By combining these strategies, this work seeks to significantly improve the performance and efficiency of CIGS solar cells.

2. Proposed Method and Electrode Structure and Role of Layers

In this research, a 1µm=1000nm wide cell has been modeled by using Silvaco Software according to the specifications in Table 1.

In the modified design of the CIGS solar cell, the ITO layer, positioned at the top of the device and exposed to direct sunlight, functions as the actual anode. In contrast, the metallic back contact (silver or molybdenum), which is in direct contact with the CIGS absorber layer, serves as the true cathode. Importantly, the Al2O3 layer is incorporated only as a thin and localized interfacial layer, using a pitch-based configuration between the CIGS and the metal contact. This layer acts as an effective passivation interface, reducing carrier recombination and enhancing electron selectivity. Therefore, Al2O3 does not serve any electrical role as a cathode in this structure and is not used as an independent electrode in any part of the device [42].

It is worth noting that the glass/SiO2 substrate in the CIGS solar cell structure acts only as a mechanical support and an electrical insulator and does not play any role in electrical conductivity. The back electrical contact is established through a molybdenum (Mo) layer deposited directly on this insulating substrate. Therefore, the presence of the SiO2 layer does not hinder the electrical contact. In Figure 7, the Mo layer is shown as the back contact. This is clearly stated in references [17 & 41] .

Table 1.Optimized Layer Structure of the CIGS Solar Cell (Bottom to Top)

Color	Reg.	Layer	Material	Type
	#1	Substrate	Glass / SiO2	Insulator
	#2	Back contact	Mo	Metal (Cathode)
	#3	Passivation layer	Al_2O_3	Insulator
	#4			
	#5			
	#6	Absorber layer	$CuInGaSe_2$	p-type semiconductor
	#7	Buffer layer	CdS	
	#8	Window layer	ZnO	Transparent n-type semiconductor
	#9	Transparent conductor	ITO	Indium Tin Oxide (Anode)
	#10	Conductor	Silver grid	Metal

The mobility values at 300°C for electrons and holes are 200 and 25 cm^2/v.s, respectively, and the stability time for electrons and holes in the buffer, absorption, and window layers is 1.5 ns.

Function Φf = 4.6 eV and surface recombination velocities for electrons and holes set to 1×10^7 cm^{-3} was used as the cathode (back contact), while indium tin oxide (ITO) with a work function Φ_a = 4.7 eV was implemented as the transparent anode. A thin aluminum oxide (Al2O3) layer (Φ = 4.3 eV) was inserted between the CIGS absorber and Mo contact as a passivation interface, not as an electrode (Table 2).

In the proposed structure, the molybdenum (Mo) layer functions as the back contact or cathode electrode, while the Al2O3 layer serves solely as a surface passivation layer with no electrical or contact role. This layer is applied locally or as a thin film with a patterned design to ensure that it does not block the electrical contact between the Mo and the CIGS absorber layer. Such an approach is fully consistent with modern solar cell design principles, particularly in CIGS and silicon technologies, and is well documented in reputable scientific literature.

Table 2. Electron and Hole recombination rate of anode and cathode.

Metal	Contact Name	Workf	VSURFN	VSURFP
ITO	transparent anode	4.7	1e7	1e7
Mo	Cathode	4.6	1e7	1e7

Therefore, the output of the software is shown in Figure 7 with the specified areas. In general, solar cells use light radiation with a standard AM1.5G spectrum at a 90-degree angle to the cell surface (Figure 8) [24-26 &35] to achieve the best result and highest efficiency.

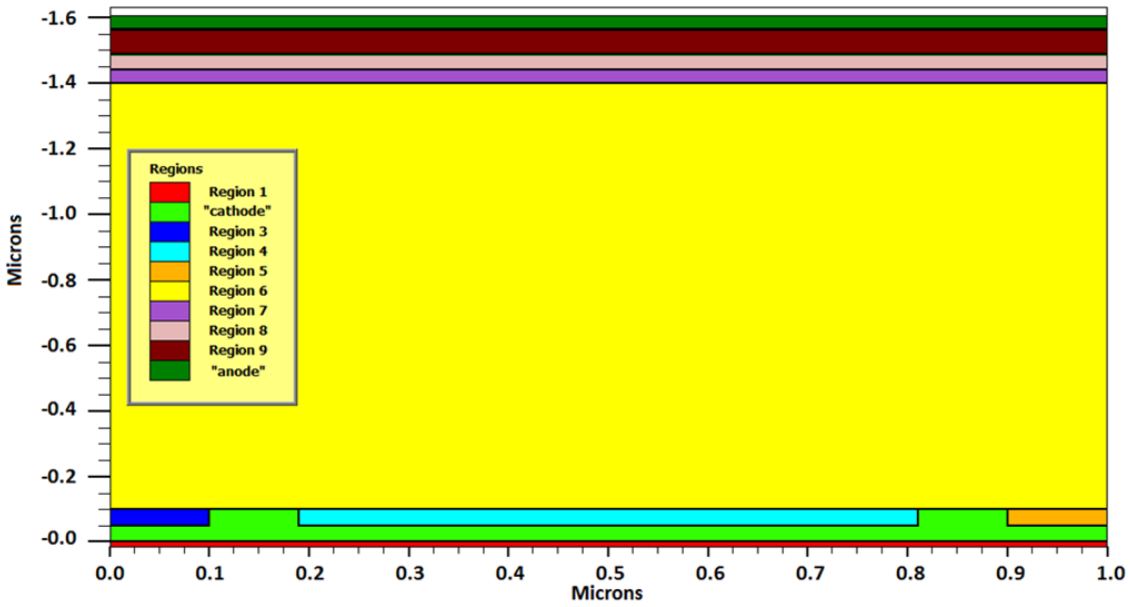

Figure 7. Required and planned areas in the research cell.

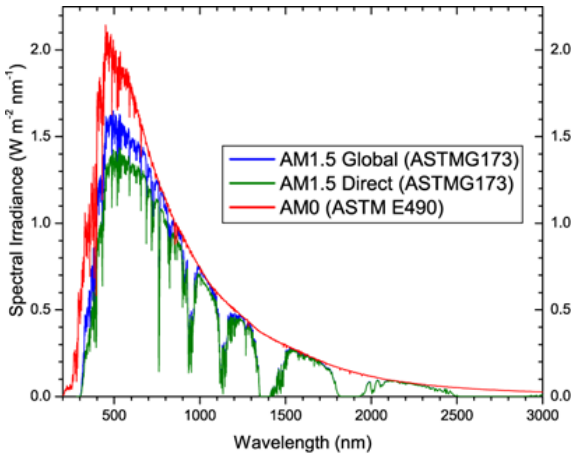

Figure 8. Standard solar spectrum for use in space and on Earth [35].

In this research, by irradiating a light spectrum with an intensity of 1.2 W/cm^2 and a radiation angle of 90 degrees according to Figure 9, currents with the values of Table 3 appear in the anode and cathode electrodes.

Table 3. Specifications of the light irradiated to the surface of the solar cell under investigation

Beam Number	Applied	$I_{sampled}$ (W/ cm^2)	I_{input} (W/cm^2)	J_{source} (A/um)	$J_{available}$ (A/um)
B=1	0.1	0.0927	0.0998	5.720e-010	3.595e-010

3. Applied Equations

The simulation of solar cells involves analyzing the principles of operation, models of electron and hole transport, recombination and carrier generation, and calculating key parameters such as open-circuit voltage

(VOC), short-circuit current (Jsc), fill factor (FF), and efficiency (η). This process utilizes equations such as Poisson's equation, continuity equations, and recombination rate equations, examining carrier transport through diffusion and drift to optimize the design and performance of the cell [27–29].

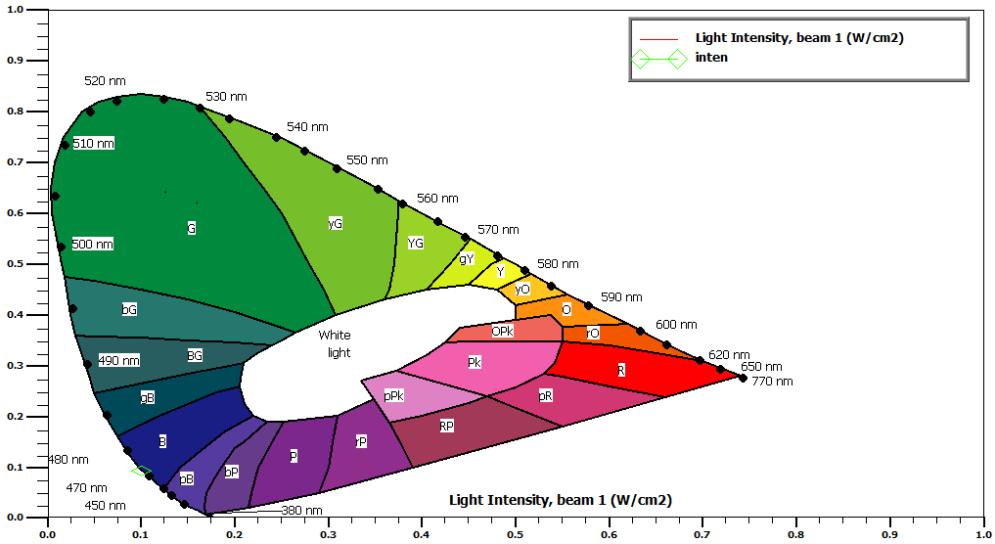

Figure 9. The spectrum of the light band irradiating the cell surface

The total cell width in the simulation is set to 1 µm, and the mesh is defined with a spatial resolution of dev = 0.1 µm, resulting in mesh lines at x = 0, 0.1, 0.2,..., 1.0 µm. This corresponds to 10 equal pitch steps, each measuring 100 nanometers, distributed uniformly across the lateral dimension. Additionally, rear openings are introduced with a lateral offset of 10 nm, enabling localized carrier extraction through the back contact. These structural features, including the regular pitch and offset scheme, are illustrated in Figure 10, supporting the rear-passivated design strategy implemented in the simulation.

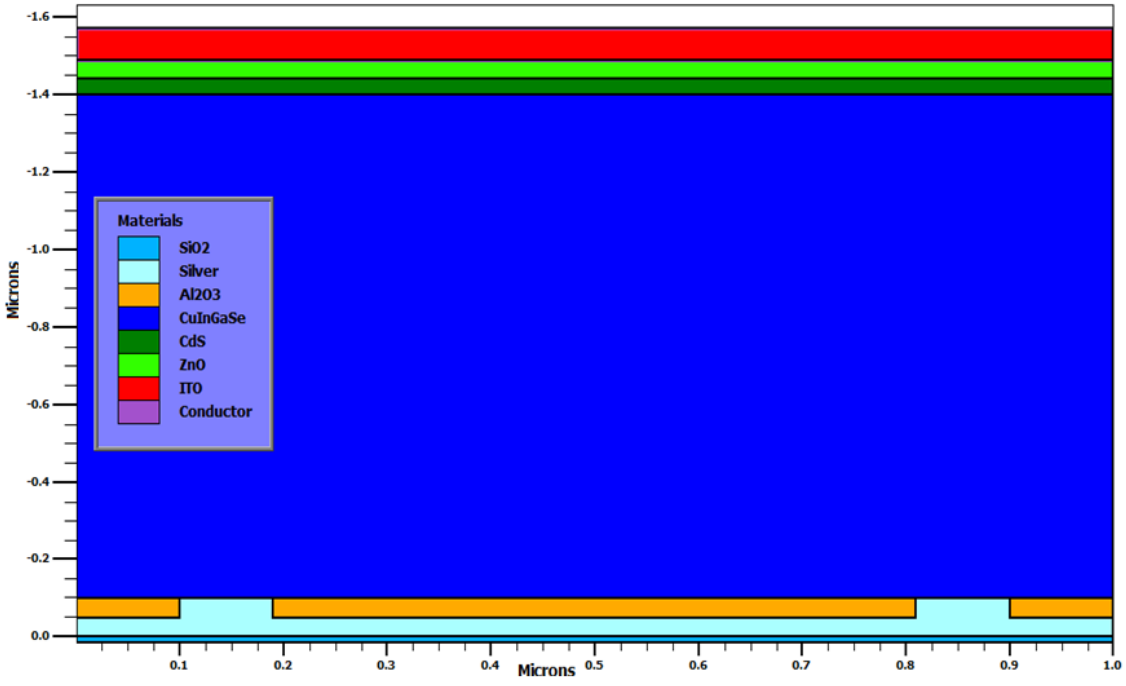

Figure 10. The investigated CIGS thin film cell components.

4. Simulation Results

Considering the weakness of CIGS thin-film elements in the back terminal (connector) due to high molybdenum resistance and conduction loss, in this study, creating a gap (Pitch) reduces the contact resistance. As a result of the potential difference, this is achieved by balancing the efficiency current and voltage (Eff). Therefore, to achieve the best result, we set the width of the Pitch from 10 nm to 90 nm, which is selected according to the degree of narrowness of the gap, and the following figures and diagrams. It is worth mentioning that the width of the gap cannot be increased more than usual, because the joint surface between the joint and damping layers should be limited. Designing this cell and specifying the materials of each layer with a thickness according to Table 4 and a channel width of 1000 nm (Number of pitches= 10), Figure 10 is extracted using Silvaco software.

$$\text{Pitch Width} = \frac{\text{Total Cell Width}}{\text{Number of pitches}} = \frac{1\ \mu\text{m}(1000\ \text{nm})}{10} = 0.1\mu\text{m} = 100\text{nm} \quad (1)$$

Table 4. Thickness and amount of gallium doping in the absorption region

Material	Mo	Al	CuInGaSe	CdS	ZnOAl	ZnO	Silver
Thickness (nm)	0.05	0.05	1.3	0.04	0.05	0.08	0.1
x.comp	-	-	0.9	-	-	-	-

The thickness of the cell components in terms of nanometers is given in Table 4, and the density and concentration of aluminum doped with zinc oxide is 1e14 cm-3. Here, the combined ratio x=Ga/((Ga+In)) of gallium and indium is chosen to be 0.9 in the best case when changing the concentration of gallium and indium, we observe changes in the band gap, For changes from x =0 to x=1, the band gap of the absorption layer varies from 1.04 ev to 1.68 ev according to the formula Eg = 1.010 + 0.626x - 0.167x(1 - x) . When the parameter x increases, the output power density increases. In Table 5, the type of semiconductor (p, n) and the density of each of the absorber, buffer, and window layers are presented, and in Table 6, the specifications and values of each of the parameters used in the cell are given. The lifetime of electrons and holes for each material listed in the table is equal to 1e- 7, (Taun0=Taup0).

Table 5. Absorber, buffer, and window layers and its p or n type.

Material	layer type	doping uniform type	concentration
CuInGaSe	absorber	p.type	1e+014
CdS	buffer	n.type	5.0e19
ZnO	window	n.type	1.0e19

Table 6. Properties and ingredients of solar cell materials.

Material	EG300	Permittivity	Affinity	Mun	Mup	Nc300	Nv300
CuInGaSe	1.15	13.6	4.8	200	25	2.2e18	1.8e19
CdS	2.4	10	4.5	100	25	2.2e18	1.8e19
ZnO	3.3	9	4.7	100	25	2.2e18	1.8e19
ITO	3.5 – 4.3			7.5			

The work function or bandwidth of the absorption layer is considered equal to EG300=1.15 to ensure the minimum energy necessary to remove an electron from the valence band and reach the conduction band. Permittivity = 13.6, the mobilities of electrons and holes for their free mobility within the semiconductor are MUN = 100 and MUP = 25, respectively. The carriers' concentration in the conduction and capacitance bands are NC300 = 2.2e18 and NV300 = 1.8e19. The lifetime of hole and electron carriers is (taup0=1e-7, taun0=1e-7). Table 7 shows the failure rates for each parameter associated with the absorber, buffer, and window layer.

Adjusting the voltage from 0 to 1.2 V in steps (step size=0.02 V) and also the pitches (10, 20, 30, 40, 60, 80, and 90nm), the diagram of anode voltage according to cathode current is obtained according to the Figure 11.

The relationship between cathode current and anode voltage (0–1.2 V, step size 0.02 V) was studied for various pitches (10–90 nm). Results show a steady increase in electron current density with voltage, while hole and cathode current densities slightly decrease. The small variation in Jc indicates its relative stability over the voltage range.

Table 7. Defect frequency for each absorber, buffer, and window layer.

Defect Density	CuInGaSe	CdS	ZnO
NTA	0	0	0
NTD	0	0	0
WTA	1	1	1
WTD	1	1	1
NGA	0	2.3E17	0
NGD	8E15	0	1e17

EGA	0.575	1.2	1.65
EGD	1E-7	1.2	1.65
WGA	1E-7	0	1
WGD	0.1	1	0.1
Sigtae	1.E-17	1.E-17	1.E-17
Sigtah	1.E-15	1.E-15	1.E-15
Sigtde	1.E-15	1.E-15	1.E-15
Sigtdh	1.E-17	1.E-17	1.E-17
Siggae	2.E-17	2.E-17	2.E-16
Siggah	2.E-12	2.E-12	2.E-15
Siggde	5.E-13	5.E-13	5.E-12
Siggdh	1.E-15	1.E-15	1.E-15

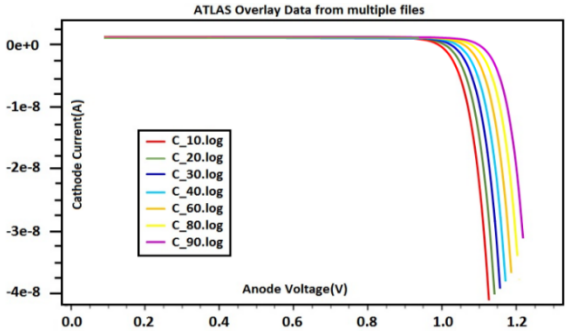

Table 8 - Current density according to different anode voltages.

Anode voltage (V)	0.0	2.0	4.0	6.0	8.0	1.0	1.2
Jn (A/µm)	6.707e-014	6.939e-014	7.182e-014	7.434e-014	7.698e-014	7.974e-014	8.263e-014
Jp(A/µm)	-3.388e-010	-3.387e-010	-3.387e-010	-3.386e-010	-3.386e-010	-3.385e-010	-3.384e-010
Jc(A/µm)	-3.38	-3.38	-3.38	-3.38	-3.38	-3.38	-3.38

Figure 11 - application of voltage to the anode in the range (0-1.2 volts).

The diagram in Figure 12 illustrates the magnification of the cathode current in terms of the anode voltage, and as the step increases, the anode voltage also increases. In this research, the voltage value of anode = 1.153 V for pitch = 90 nm .Table 8 shows the current density values at different anode voltages, illustrating their relationship.

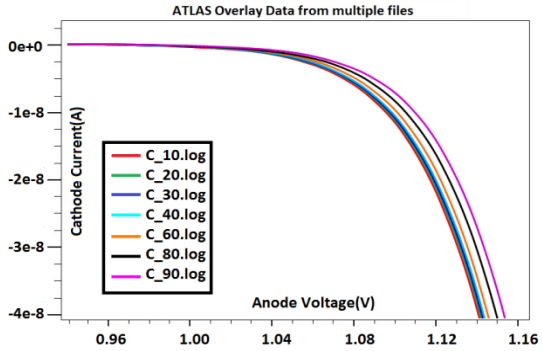

Figure 12. Voltage gain from 0.0 to 1.2 volts at various pitch levels 10, 20, 30, 40, 60, 80 and 90 nm.

	7e-010	7e-010	6e-010	5e-010	5e-010	4e-010	4e-010
Jt(A/µm)	-3.387e-010	-3.387e-010	-3.386e-010	-3.385e-010	-3.385e-010	-3.384e-010	-3.384e-010

figure 13 shows the structure of the CIGS solar cell for pitch values ranging from 10 to 90 nm.As the pitch decreases, contact channels become closer and rear openings more dense, enhancing carrier extraction but potentially increasing contact résistance. In contrast, larger pitches reduce contact area, which can limit current collection. These structural changes directly affect the cell's electrical performance, including resistance, recombination, and current extraction efficiency.

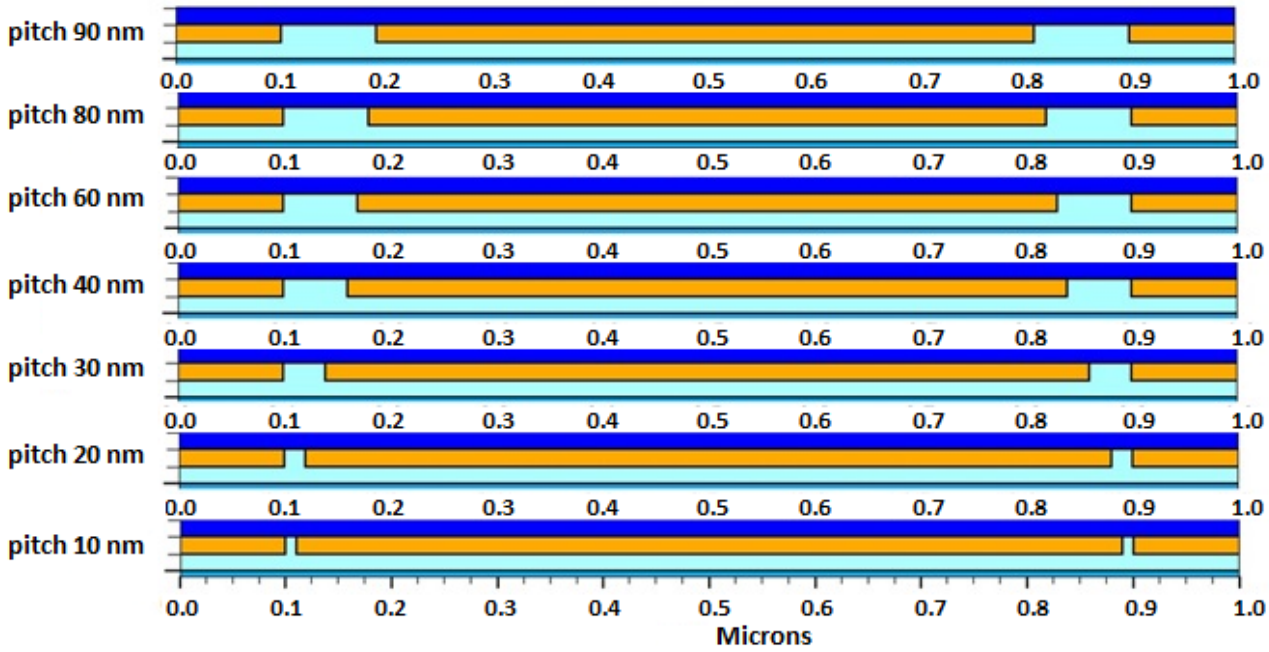

Figure 13. CIGS cell structure with different channel widths.

The effect of pitch on the efficiency of CIGS solar cells refers to adjusting the distance between cells, which can improve light absorption, carrier transport, and overall cell performance. By optimizing the pitch, light absorption increases, optical losses are reduced, and carrier transport improves, leading to higher efficiency. Additionally, material and structural alignment can reduce defects and enhance performance. For instance, the cell structure of the CIGS thin layer for pitch = 10 is similar to that shown in Figure 10, but changing the channel width produces a structure similar to Figure 13, where the designed cell width is 1 μm(1000 nm). The smaller the channel width, the higher the anode voltage, as demonstrated in Figure 13

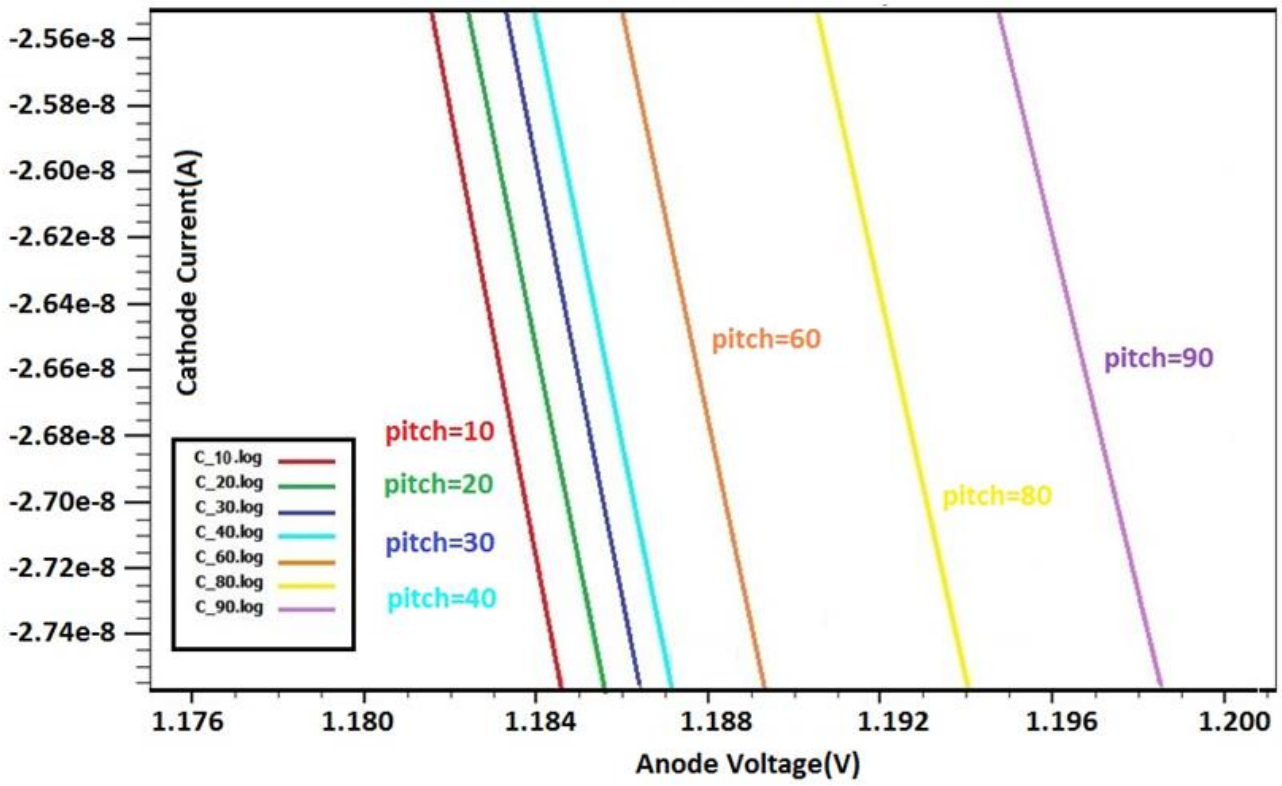

Figure 14. Voltage gain from 0.0 to 1.2 volts at various pitch levels 10, 20, 30, 40, 60, 80, and 90 nm.

In Figure 14 analyzes the voltage gain of CIGS solar cells across different pitch widths from 10 to 90 nm. It shows that smaller pitches (10–20 nm) result in steeper voltage curves due to higher contact resistance. Larger pitches (80–90 nm) yield slower voltage increases and lower final voltages. The best voltage output occurs at a pitch of around 20 nm. This highlights the importance of pitch optimization in enhancing solar cell efficiency through structural design.

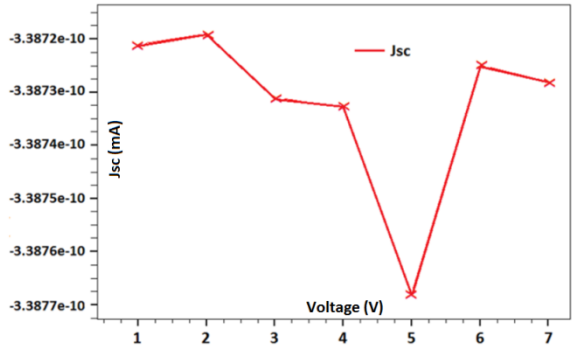

Figure 15. Jsc short circuit current density diagram at different heights.

In the diagram shown in Figure 15, the short-circuit current density is almost at a maximum value for the channel with a width of Pitch=20 and reaches a minimum value at Pitch=50 and then increases and the best case occurred at Pitch=20.

As shown in the figure, the thickness of the absorber layer plays a crucial role in determining the short-circuit current density. The highest short-circuit current density occurs at Pitch=20 due to the optimal combination of absorber layer thickness and channel width, maximizing light absorption and minimizing carrier recombination. Variations in absorber layer thickness significantly affect device performance.

Decreasing the width of the channels has caused an increase in the potential difference and then an increase in the value of the open circuit voltage, and as can be seen in Figure 16, as we move from a smaller width (pitch=10nm) to a higher width (pitch=90nm), V_{OC} also increases. In figure 16, the potential difference between the anode and the cathode increased. If we connect the pitch directly to the absorbent layer, the potential difference will drop drastically. So we are not allowed to lower the open circuit voltage below a certain limit. Changing the width of the gap (pitches) is to create a balance between the current and the voltage of the cell, which means that the voltage cannot drop too much, and on the other hand, we should not have too much current. The diagram in Figure 16 shows that the smaller the pitch width (the narrower the opening of the gap), the higher the contact resistance of the back connection, resulting in the voltage difference increases and the V_{OC} increases.

Decreasing the channel width increases contact resistance and open-circuit voltage, but if it becomes too narrow, the voltage drops sharply. Thus, a balance between voltage and current must be maintained for optimal cell performance.

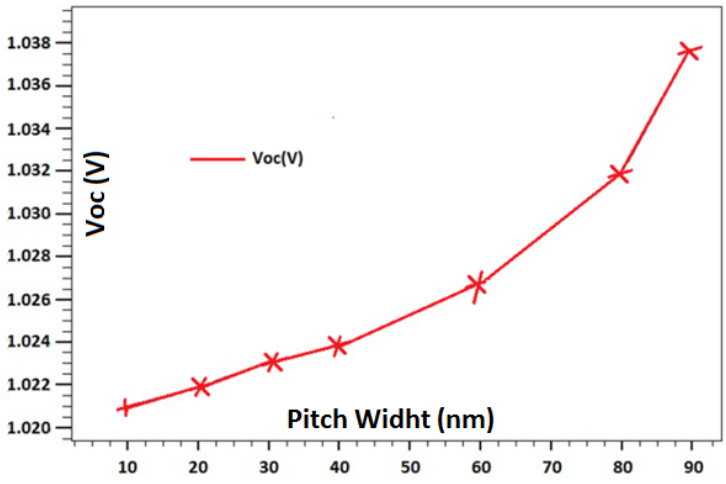

Figure 16. Effect of channel width on open circuit voltage V_{OC}.

The fill factor FF=(V_{MP}.I_{MP})/(VOC.ISC) = (Area A)/(Area B) is defined as the ratio of the maximum power (VMP.IMP) to the product of the short circuit current and open circuit voltage (V_{OC}.I_{SC}). This factor in solar cells depends on the temperature and the structure of the element. Figure 17, for all types of solar cells, depicts the output power diagram of cells with two levels A and B (red line), and the input power (blue line) versus the cell short circuit current (I_{sc}), open circuit voltage (V_{OC}) and maximum power point (V_{mp}, $I_{m/p}$) [31]. The results of this study in Figure 18 show the fill factor (FF).

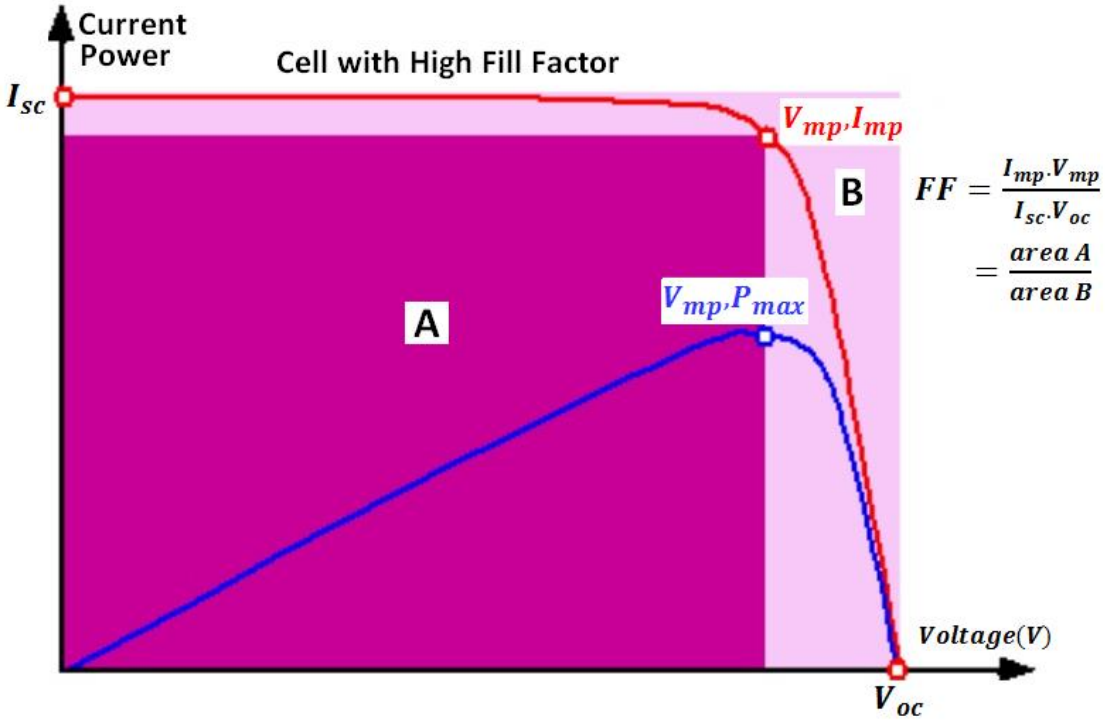

Figure 17. Solar cell fill factor[31]

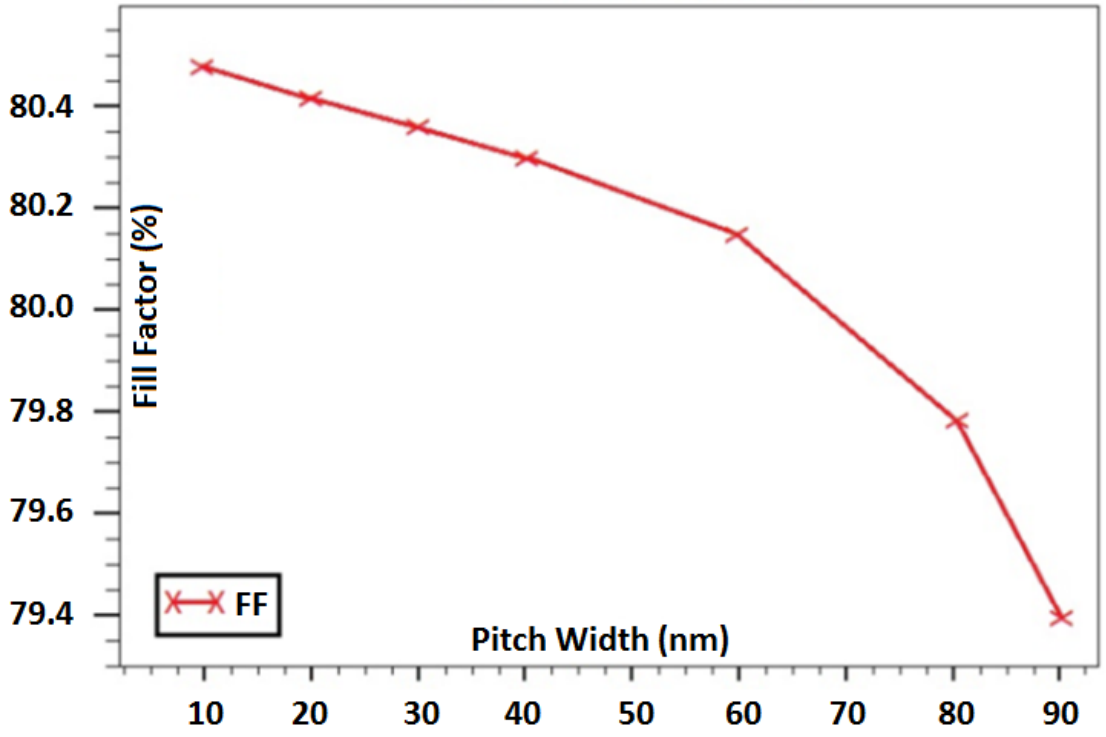

Figure 18. Fill factor for different pitches.

The amount of filling is directly related to the decrease or increase of the width of the channel, which means that

when the width of the pitch decreases, the amount of filling is also decreased, and the reason for this is the increase of the channel open circuit voltage in wider channels, as shown in Figure 16. As the channel width narrows, its penetration into the connector is limited, and as a result, the fill factor decreases.

In this study, the following formula EQE= (amount of input light)/ (total recombination) = Frad/ (Frad+Fau+Fsrh) is used to calculate the gain and efficiency, where EQE is equal to the incident light ratio to the total amount of reflected light in a solar cell.

The external quantum efficiency EQE (λ) is the ratio of the number of charge carriers collected by the solar cell to the number of photons that radiate from the outside of the solar cell with a certain energy and wavelength (random photons), EQE (λ) = (Number of collected electrons)/ (Number of incident photons) = (I (λ)/q)/ (φP (λ)), [32].

As the extension is created and the gap width changes, the efficiency varies. The narrower the gaps become, the greater the efficiency gain, because the open circuit voltage increases (Figure 19). With a pitch of 90 µm, the highest efficiency is obtained. The studied cell design parameters and results are as follows:

J_o = -1.24623e-09, J_{sc} (mA/cm²) = -62.3115 , V_{OC} = 0.690475 , P_m = -7.02303e-10 , V_m = 0.6(V) , I_m = -1.17051e-09(mA) , FF = 81.6166(%) , Efficiency = 35.1151.

Table 9 compares the results of this study with findings from existing similar works, highlighting similarities and differences. Table 10 compares the cell structure and simulation methods of this study with those used in previous works. Table 11 compares the performance of CIGS solar cells with and without the ITO layer, highlighting the impact of the layer on efficiency.

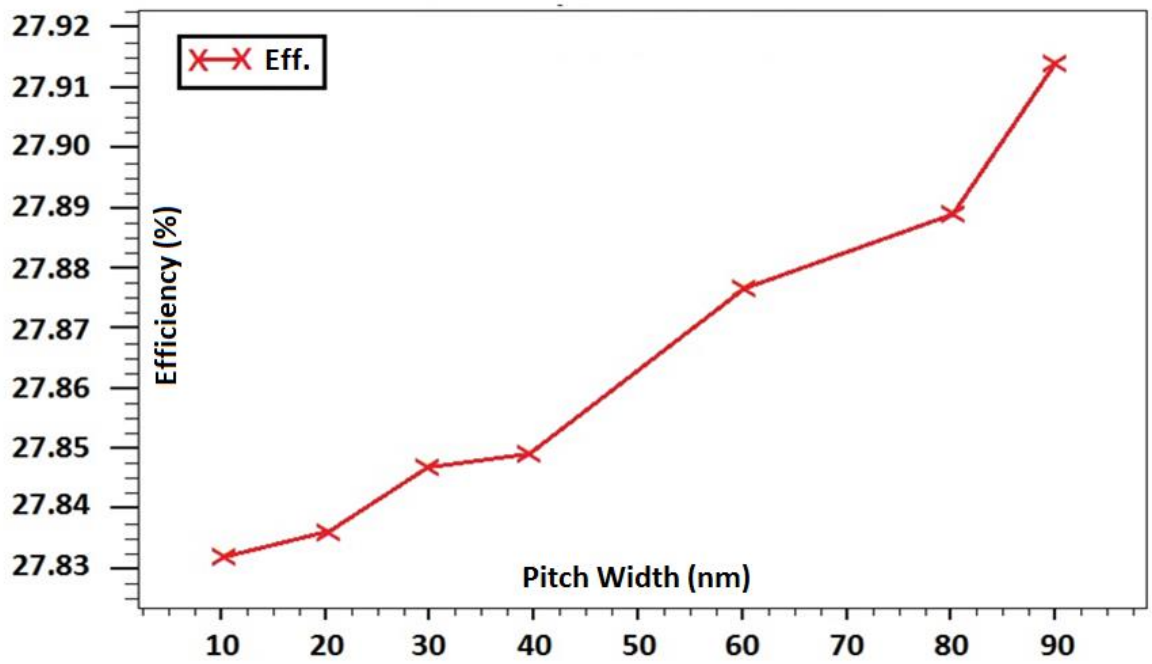

Figure 19. Increase in interest due to changing the width of the channels.

Table 9. Comparison table of this work and existing similar works.

Reference	Eff. (%)	Voc(V)	Jsc (mA/cm^2)	FF (%)
[32]	9.77	0.72	30	70
[33]	17.8	0.74	34.8	75
[34]	23.64	0.74	36.4	76
[12]	14.3	0.76	31.42	74.6
This work	27.5	0.69	62.3	81.6

Table 10. Comparison table of the cell structure and software/simulation method of several studies with this work.

Reference	Cell Structure	Software /Simulation Method
[12]	CIGS/CdS/ZnO/Glass	Silvaco-TCAD
[32]	CIGS/CdS/ZnO/Glass (with optimized absorber layer thickness and gallium distribution)	Silvaco-TCAD
[33]	CIGS Thin-Film	No specific software method (focus on material properties and fabrication techniques)
[34]	CIGS with ITO Front Contact	Experimental Methods (simulation not explicitly mentioned)
This work	CIGS/CdS/ZnO/pitch	Silvaco-TCAD

Although transparent conductive oxides (TCOs) are widely considered cost-effective alternatives to indium tin oxide (ITO) due to their transparency, conductivity, mechanical strength, and lower production costs, ITO remains the preferred choice in this study. Its superior electrical conductivity, high transparency in the visible spectrum, greater chemical and thermal stability, and excellent compatibility with the fabrication of ultra-thin, multi-layered solar cells make it particularly suitable. Moreover, employing ITO as the front photoanode reduces series resistance and enhances overall device efficiency. Fan et al. (2023) further confirmed that precise control over ITO layer thickness significantly improves optical and electrical properties, reinforcing its effectiveness as a high-performance TCO [40].

Table 11. Comparison of the performance of CIGS solar cells in two states, with and without the ITO & pitch layer.

Ref. No.	Solar Cell Structure	FF (%)	Voc (V)	Jsc (mA/cm²)	Eff. (%)
[36]	Standard CIGS	68.0	0.65	34.0	15.2
[37]	CIGS with ITO layer	75.0	0.72	36.5	23.0
[38]	CIGS with pitch at back layer	70.0	0.69	35.2	15.0
New Results	CIGS with ITO & pitch at back layer	81.6	0.69	62.3	27.5

In study [36], the use of a standard CIGS structure with ZnO/CdS layers and full contact with Mo exhibited limited performance due to high carrier recombination rates at both the front and back regions, as shown in Table 11. In [37], the introduction of a transparent ITO layer enhanced light transmittance and reduced series resistance, resulting in lower carrier recombination and significant improvements in electrical and optical performance. In [38], carrier recombination was further reduced by applying a back-side patterning structure with a pitch of 1.5 μm and openings of 300 nm, leading to a moderate enhancement in device performance. Finally, as evidenced by the new results summarized in Table 11, the simultaneous implementation of front-side transparency enhancement via ITO and back-side recombination control through pitch structuring led to a remarkable improvement in cell efficiency.

The utilization of a pitch structure at the back contact was previously investigated in the study by Boukortt et al. [Solar Energy, 2024]. In the present work, in addition to optimizing the back pitch structure to further reduce carrier recombination, a new innovation has been introduced. Specifically, an ITO layer has been incorporated as a front electrode to enhance light collection and reduce series resistance—an improvement that was not considered in the work of Boukortt et al.The comparison between the results of the new research and the findings of Boukortt et al. (2024) is summarized in Table 12 below.

Table 12: Performance Comparison of the New Research Results with the Findings of Boukortt et al. (2024)

Feature	**Boukortt et al. [Reference]**	**New Research**
Front Layer Structure	ZnO/CdS (no ITO layer)	ITO/CdS/ZnO (adding a transparent ITO layer)
Structural Improvements	Only Pitch at back	ITO at front + Pitch at back
Short-Circuit Current ,JSC (mA/cm²)	35.2	62.3
Open-Circuit Voltage ,VOC (V)	0.68	0.69
Fill Factor (FF) (%)	70.0	81.6

Power Conversion Efficiency ,PCE, (%)	15.0	27.5
Carrier Recombination Rate	Moderate (reduction only by pitch)	Low (through dual improvement)

This study significantly improved the performance of CIGS solar cells by optimizing the back contact spacing and using a transparent ITO electrode on the front layer. According to Table 12, these changes reduced internal resistance and carrier recombination, increasing the cell efficiency from 15% to 27.5%. The results indicate that combining these two methods is an effective approach to enhance the efficiency and stability of solar cells.

In the study by Boukortt et al., optimization of the back pitch structure alone resulted in a power conversion efficiency (PCE) of 15%, limited by moderate carrier recombination. In contrast, the new research introduces a dual optimization strategy. The addition of an ITO layer as a front electrode improves optical transparency and reduces series resistance, enhancing both $\mathbf{J_{SC}}$ and $\mathbf{V_{OC}}$. Additionally, the optimized back pitch structure reduces rear surface recombination, improving $\mathbf{J_{SC}}$ and FF. This combined approach leads to a significant increase in PCE to 27.5%, representing an over 80% improvement in device performance. Our new design, through the synergistic combination of front and back optimizations, greatly enhances the performance of ultrathin CIGS solar cells.

4.1. Sensitivity Analysis Summary

A comprehensive sensitivity analysis was performed to evaluate the impact of key design parameters such as pitch width, gallium doping ratio, carrier mobility, and front/back layer structure on the performance of CIGS thin-film solar cells. The results indicate that optimizing the pitch to approximately 20 nm and adjusting the Ga/(Ga+In) ratio to 0.9 significantly enhance device efficiency. Furthermore, the integration of an ITO front electrode and a structured pitch-based rear contact collectively improves light absorption, charge transport, and recombination suppression, yielding a maximum efficiency of 27.5%.

table13: Effect of Pitch Variation on Cell Performance

Pitch (nm)	Voc (V)	Jsc (mA/cm²)	FF (%)	Efficiency (%)
10	↑0.75	↓58.4	↑82.1	26.7
20	↑0.73	↑62.3	↑81.6	27.5
40	0.71	59.1	80.2	25.4
60	0.70	60.2	79.4	25.8
90	↓0.69	57.5	78.5	24.6

Pitch (nm)	Voc (V)	Jsc (mA/cm²)	FF (%)	Efficiency (%)
Result	Optimum pitch width for maximum efficiency ≈ 20 nm			

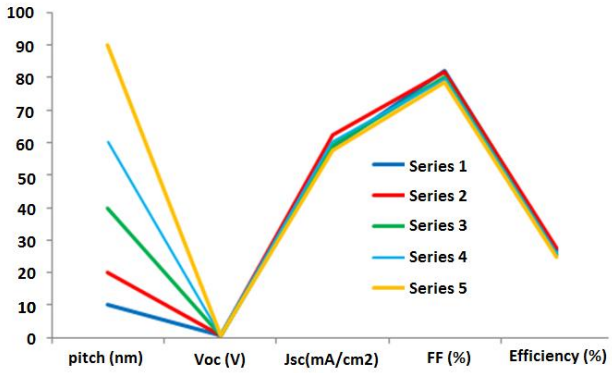

Figure 20. Impact of ITO and Pitch on Solar Cell Performance Parameters.

Figure 20 shows the impact of pitch width variation on the performance of CIGS solar cells. According to Table 13, pitch size significantly affects key parameters such as Voc, Jsc, FF, and efficiency. At very small pitches (10 nm), Voc and FF are high, but reduced light absorption leads to a drop in Jsc and overall efficiency. Conversely, at larger pitches (e.g., 60 and 90 nm), Jsc may improve slightly, but lower Voc and FF reduce performance.The maximum efficiency of 27.5% is achieved at a pitch of 20 nm, indicating an optimal balance between light management and recombination suppression. These findings highlight that precise pitch engineering is crucial for maximizing solar cell performance.

Table 14: Effect of Ga/(Ga+In) Ratio in the Absorber Layer (x-comp):

x (Ga/(Ga+In))	Bandgap Eg (eV)	Voc (V)	Jsc (mA/cm²)	Efficiency (%)
0.0	1.04	0.61	68.5	25.5
0.3	1.23	0.65	66.1	26.2
0.6	1.47	0.68	64.0	26.8
0.9 (optimum)	1.63	0.69	62.3	27.5
1.0	1.68	0.70	60.1	26.5
Result	Optimal performance occurs at x = 0.9, with a balance between voltage and current			

Table15: Effect of Carrier Motilities on Efficiency

μn (cm²/V•s)	μp (cm²/V•s)	Voc (V)	FF (%)	Efficiency (%)
100	25	0.68	79.5	25.9
150	25	0.69	80.2	26.8
200	25 (baseline)	0.69	81.6	27.5

μn ($cm^2/V•s$)	μp ($cm^2/V•s$)	Voc (V)	FF (%)	Efficiency (%)
250	30	0.70	82.1	28.0
300	35	0.71	82.4	28.4
Result	Increasing carrier mobility improves efficiency and reduces internal resistance.			

Table16: Effect of Including/Excluding ITO and Pitch Structures

Structure Type	Voc (V)	Jsc (mA/cm^2)	FF (%)	Efficiency (%)
No ITO & Pitch	0.62	53.7	73.2	20.8
Only Pitch	0.67	59.2	78.4	24.5
Only ITO	0.65	60.1	79.0	25.4
ITO + Pitch	0.69	62.3	81.6	27.5
Result	Combining both ITO and pitch significantly reduces recombination rate and increases performance			

Table17: Performance Comparison of CIGS Solar Cells with Different Structural Configurations: Effect of ITO and Rear Pitch Design.

Structure Type	Voc (V)	Jsc (mA/cm^2)	FF (%)	Efficiency (%)
No ITO & Pitch	0.62	53.7	73.2	20.8
Only Pitch	0.67	59.2	78.4	24.5
Only ITO	0.65	60.1	79.0	25.4
ITO + Pitch	0.69	62.3	81.6	27.5
Result	Combining both ITO and pitch significantly reduces recombination rate and increases performance			

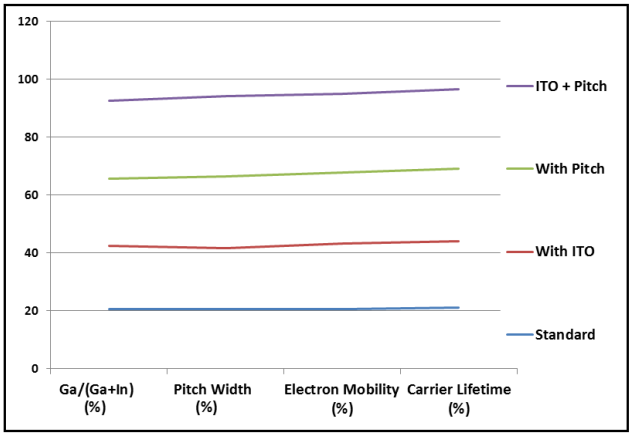

Figure 21: Sensitivity analysis of key parameters in CIGS solar cells

Figure 21 presents the sensitivity analysis of key performance parameters in CIGS solar cells. The results align with Table 17, indicating that the simultaneous use of the ITO layer and rear pitch design reduces recombination rates and enhances parameters such as Voc, Jsc, FF, and overall efficiency. This combination improves cell efficiency from 20.8% to 27.5%, highlighting its significant role in optimizing device structure.

Table 18: Sensitivity Analysis of Key Parameters in CIGS Solar Cells

Solar Cell Structure	Ga/(Ga+In) (%)	Pitch Width (%)	Electron Mobility (%)	Carrier Lifetime (%)
Standard	20.5	20.5	20.5	21
With ITO	22	21	22.8	23
With Pitch	23	25	24.5	25
ITO + Pitch	27	27.5	27.2	27.5

4.2. Challenges and Complexities of the Pitch Structure in Solar Cells

The fabrication process and implementation of the pitch structure involve selecting appropriate materials, precision in measurements, and utilizing advanced manufacturing techniques such as lithography. Its complexities include precise coordination between layers, high accuracy in adjusting the pitch distance, and scalability challenges. In real-world applications, challenges such as high costs, the need for durability in various environmental conditions, and flexibility for use in diverse environments arise. These factors make the fabrication and implementation of the pitch structure require careful attention, suitable materials, and advanced techniques [30 & 39].

5. Conclusions

This paper investigated innovative approaches to improve the efficiency of CIGS chalcopyrite thin film solar cells and using advanced techniques and optimization in layer design, including the use of ITO anti-reflection layer, back layer, and material doping, solar cell efficiency increased significantly. Significant results include increased short-circuit current, reduced back-end resistance, improved conductivity, and increased open-circuit voltage (V_{OC}). The obtained values show an increase in the efficiency of conventional CIGS solar cells from about 20.8% for the optimized cell to 27.5%, which is an important advance in the field of solar energy technology. This development not only creates new horizons for clean energy production, but is considered an important step to reduce dependence on fossil energy sources and curb climate change. The ITO layer and pitch significantly impact the efficiency of CIGS solar cells:

ITO Layer: in this study, ito (indium tin oxide) was chosen for its high conductivity and optical transparency, making it ideal for ultrathin cigs solar cells. its excellent transparency in the visible light range enhances light absorption, reduces optical losses, and improves charge carrier collection, resulting in higher efficiency. ito's stability and compatibility with cigs fabrication processes further optimize performance. while tco is more cost-effective, ito was selected for its superior ability to improve the performance of cigs solar cells, making it the most suitable choice for the specific design and goals of this research [23].

Pitch: The distance between electrodes affects electron transport, with larger pitch increasing losses. Proper pitch helps with uniform current distribution and better interaction with the active layer, improving efficiency [31].

Optimizing both parameters enhances conductivity, light absorption, and charge collection, thereby improving the overall efficiency of CIGS solar cells.

References

[1] A. Chirilă et al., "Potassium-induced surface modification of Cu(In,Ga)Se2 thin films for high-efficiency solar cells," Nature Materials, vol. 12, no. 12. Springer Science and Business Media LLC, pp. 1107–1111, Nov. 03, 2013. doi: 10.1038/nmat3789.

[2] P. Jackson, R. Wuerz, D. Hariskos, E. Lotter, W. Witte, and M. Powalla, "Effects of heavy alkali elements in Cu(In,Ga)Se2 solar cells with efficiencies up to 22.6%," physica status solidi (RRL) – Rapid Research Letters, vol. 10, no. 8. Wiley, pp. 583–586, Jul. 12, 2016. doi: 10.1002/pssr.201600199.

[3] B. G. PRIYADARSHINI and A. K. SHARMA, "Design of multi-layer anti-reflection coating for terrestrial solar panel glass," Bulletin of Materials Science, vol. 39, no. 3. Springer Science and Business Media LLC, pp. 683–689, May 26, 2016. doi: 10.1007/s12034-016-1195-x.

[4] J. Chantana, T. Kato, H. Sugimoto, and T. Minemoto, "Heterointerface recombination of Cu(In,Ga)(S,Se)2,based solar cells with different buffer layers," Progress in Photovoltaics: Research and Applications, vol. 26, no. 2. Wiley, pp. 127–134, Nov. 03, 2017. doi: 10.1002/pip.2952.

[5] I. Gharibshahian, S. Sharbati, and A. A. Orouji, "Potential efficiency improvement of Cu (In, Ga) Se2 thin-film solar cells by the window layer optimization," Thin Solid Films, vol. 655. Elsevier BV, pp. 95–104, Jun. 2018. doi: 10.1016/j.tsf.2018.04.014.

[6] S. Sharbati, I. Gharibshahian, and A. A. Orouji, "Designing of AlxGa1-xAs/CIGS tandem solar cell by analytical model," Solar Energy, vol. 188. Elsevier BV, pp. 1–9, Aug. 2019. doi: 10.1016/j.solener.2019.05.074.

[7] J. F. Guillemoles, "The puzzle of Cu(In,Ga)Se2 (CIGS) solar cells stability," Thin Solid Films, vol. 403–404. Elsevier BV, pp. 405–409, Feb. 2002. doi: 10.1016/s0040-6090(01)01519-x.

[8] A. Bahrami, S. Mohammadnejad, N. J. Abkenar, and S. Soleimaninezhad, "Optimized Single and Double Layer Antireflection Coatings for GaAs Solar Cells," International Journal of Renewable Energy Research, vol. 3, no. 1, pp. 79–83, Mar. 2013.

[9] G. Sozzi *et al*., "Designing CIGS solar cells with front-side point contacts," in *2015 IEEE 42nd Photovoltaic Specialist Conference (PVSC)*, New Orleans, LA, USA, Jun. 2015, pp. 1–5, doi: 10.1109/PVSC.2015.7355691.

[10] A. Khadir, A. Kouzou, and M. K. Abdelhafidi, "Effect of Anti-Reflective Coating on CIGS Solar Cells Performance," 2020 17th International Multi-Conference on Systems, Signals & Devices (SSD). IEEE, Jul. 20, 2020. doi: 10.1109/ssd49366.2020.9364175.

[11] N. E. I. Boukortt, M. Adouane, and R. AlHammadi, "High-performance ultrathin Cu(In,Ga)Se2 solar cell optimized by silvaco tools," Solar Energy, vol. 228. Elsevier BV, pp. 282–289, Nov. 2021. doi: 10.1016/j.solener.2021.09.072.

[12] N. E. I. Boukortt, S. Patanè, and Y. M. Abdulraheem, "Numerical investigation of CIGS thin-film solar cells," Solar Energy, vol. 204. Elsevier BV, pp. 440–447, Jul. 2020. doi: 10.1016/j.solener.2020.05.021.

[13] B. Boroomandnasab and M. H. Zolfaghari, "Optimization of CIGS/CIGS tandem solar cells by adjusting layer thickness using Silvaco-TCAD," J. Green Eng. Renewable Innov., vol. 1, no. 1, pp. 48–58, 2024, doi: 10.61186/jgeri.1.1.48.

[14] M. Nakamura, K. Yamaguchi, Y. Kimoto, Y. Yasaki, T. Kato, and H. Sugimoto, "Cd-free Cu(In,Ga)(Se,S)$_2$ thin-film solar cell with record efficiency of 23.35%," IEEE J. Photovoltaics, vol. 9, no. 6, pp. 1863–1867, Nov. 2019, doi: 10.1109/JPHOTOV.2019.2937218.

[15] Y. Z. Hamri et al., "Improved efficiency of Cu(In,Ga)Se2 thinfilm solar cells using a buffer layer alternative to CdS," Solar Energy, vol. 178. Elsevier BV, pp. 150–156, Jan. 2019. doi: 10.1016/j.solener.2018.12.023.

[16] N. E. I. Boukortt and S. Patanè, "Single junction-based thin-film CIGS solar cells optimization with efficiencies approaching 24.5 %," Optik, vol. 218. Elsevier BV, p. 165240, Sep. 2020. doi: 10.1016/j.ijleo.2020.165240.

[17] F. Ghamsari-Yazdel and A. Fattah, "Performance enhancement of CIGS solar cells using ITO as buffer layer," Micro and Nanostructures, vol. 168. Elsevier BV, p. 207289, Aug. 2022. doi: 10.1016/j.micrna.2022.207289.

[18] B. Vermang, J. T. Wätjen, V. Fjällström, F. Rostvall, M. Edoff, R. Kotipalli, F. Henry, and D. Flandre, "Employing Si solar cell technology to increase efficiency of ultra-thin Cu(In,Ga)Se2 solar cells," Prog. Photovolt: Res. Appl., vol. 22, no. 10, pp. 1023–1029, 2014, doi: 10.1002/pip.2527.

[19] W. J. Maeng, D.-W. Choi, J. Park, and J.-S. Park, "Indium oxide thin film prepared by low temperature atomic layer deposition using liquid precursors and ozone oxidant," *J. Alloys Compd.*, vol. 649, pp. 216–221, Nov. 2015, doi: 10.1016/j.jallcom.2015.07.150.

[20] J. A. Oke and T.-C. Jen, "Atomic layer deposition thin film techniques and its bibliometric perspective," The International Journal of Advanced Manufacturing Technology, vol. 126, no. 11–12. Springer Science and Business Media LLC, pp. 4811–4825, May 05, 2023. doi: 10.1007/s00170-023-11478-y.

[21] Hertwig, Ramis Uwe, "Investigation of interface and device properties in Cd-free CIGS thin film solar cells with vapor and plasma deposited ZnMgO buffer layers," ETH Zurich, 2022. doi: 10.3929/ETHZ-B-000597834.

[22] A. Bendoumou, A. Raidou, A. Fahmi, M. Lharch, and M. Fahoume, "Numerical Simulation: Toward High-Efficiency CIGS Solar Cell Through Buffer Layer Replacement," Lecture Notes in Electrical Engineering. Springer Nature Singapore, pp. 139–150, 2023. doi: 10.1007/978-981-19-6223-3_16.

[23] I. Gharibshahian, A. A. Orouji, and S. Sharbati, "Effectiveness of band discontinuities between CIGS absorber and copper-based hole transport layer in limiting recombination at the back contact," Materials Today Communications, vol. 33. Elsevier BV, p. 104220, Dec. 2022. doi: 0.1016/j.mtcomm.2022.104220.

[24] G. Kinsey, M. Boyd, M. Braga, and N. Riedel-Lyngskær, "Impact of global measured spectrum variation on solar photovoltaic efficiencies," OSF Preprints, Sep. 2021, doi: 10.31224/osf.io/t5hu3.

[25] A. Komilov, "Gallium content-dependent efficiency limits of CIGS solar cells at AM1.5G solar irradiance," Journal of Photonics for Energy, vol. 11, no. 03. SPIE-Intl Soc Optical Eng, Aug. 06, 2021. doi: 10.1117/1.jpe.11.035501.

[26] M. Mostefaoui, H. Mazari, S. Khelifi, A. Bouraiou, and R. Dabou, "Simulation of High Efficiency CIGS Solar Cells with SCAPS-1D Software," Energy Procedia, vol. 74. Elsevier BV, pp. 736–744, Aug. 2015. doi: 10.1016/j.egypro.2015.07.809.

[27] A. H. H. Khan and Y.-C. Wang, "Drift-diffusion modeling-guided interface optimization in BaHfS3 chalcogenide perovskite solar cells," Solar Energy Mater. Solar Cells, vol. 294, p. 113889, Jan. 2026, doi: 10.1016/j.solmat.2025.113889.

[28] R. Gottschalg, D. G. Infield, and M. J. Kearney, "Experimental study of variations of the solar spectrum of relevance to thin film solar cells," Solar Energy Materials and Solar Cells, vol. 79, no. 4. Elsevier BV, pp. 527–537, Sep. 2003. doi: 10.1016/s0927-0248(03)00106-5.

[29] H. I. Abdalmageed, M. Fedawy, and M. H. Aly, "Effect of absorber layer bandgap of CIGS-based solar cell with (CdS/ZnS) buffer layer," Journal of Physics: Conference Series, vol. 2128, no. 1. IOP Publishing, p. 012009, Dec. 01, 2021. doi: 10.1088/1742-6596/2128/1/012009.

[30] S. Q. Liew and K.-K. Chong, "Comprehensive Modelling for Analyzing the Power Conversion Efficiency of Polycrystalline Silicon Photovoltaic Device under Indoor Operating Conditions," IOP Conference Series: Materials Science and Engineering, vol. 1278, no. 1. IOP Publishing, p. 012001, Feb. 01, 2023. doi: 10.1088/1757-899x/1278/1/012001.

[31] S. Dabbabi, T. B. Nasr, and N. Kamoun-Turki, "Parameters optimization of CIGS solar cell using 2D physical modeling," Results in Physics, vol. 7. Elsevier BV, pp. 4020–4024, 2017. doi: 10.1016/j.rinp.2017.06.057.

[32] A. AlAmri, F. Bouhjar, and K. Bouhadiba, "Investigation and Optimization of Ultrathin Cu(In,Ga)Se2 Solar Cells by Silvaco-TCAD Tools," Journal of Materials Science: Materials in Electronics, vol. 32, no. 4, pp. 1323–1330, 2021. doi: 10.1007/s10854-021-06661-4.

[33] "Research on Copper Indium Gallium Selenide (CIGS) Thin-Film Solar Cells," E3S Web of Conferences, vol. 267, 2021. doi: 10.1051/e3sconf/202126702031.

[34] A. Kumar, A. K. Goyal, U. Gupta, Tanya, N. Gupta, and R. Chaujar, "Increased Efficiency of 23% for CIGS Solar Cell by Using ITO as Front Contact," Journal of Renewable and Sustainable Energy, vol. 12, no. 4, Art. 043501, 2020. doi: 10.1063/5.0012060.

[35] G. A. Farias-Basulto, M. Á. Sevillano-Bendezú, M. Riedel, M. Khenkin, and J. A. Töfflinger, "Measurement and analysis of annual solar spectra at different installation angles in central Europe," *Solar Energy*, vol. 266, Nov. 2023, Art. no. 112175, doi: 10.1016/j.solener.2023.112175.

[36] Ramanathan, K., Teeter, G., Keane, J. C., & Noufi, R. (2005). Properties of high-efficiency CuInGaSe2 thin film solar cells. Thin Solid Films, 480-481, 499–501. https://doi.org/10.1016/j.tsf.2004.11.050.

[37] M. A. Green, "Thin-film solar cells: Review of the present and future," *Solar Energy Mater. Solar Cells*, vol. 92, no. 6, pp. 741–751, 2008, doi: 10.1016/j.solmat.2007.11.004.

[38] S. H. Yang, Y. H. Lee, H. S. Kim, et al., "Effect of transparent conductive oxide layers on the performance of CIGS thin-film solar cells," *Solar Energy Mater. Solar Cells*, vol. 93, no. 7, pp. 1027–1032, 2009, doi: 10.1016/j.solmat.2009.02.010.

[39] K. Stokes, K. Clark, D. Odetade, and M. Hardy, "Advances in lithographic techniques for precision nanostructure fabrication in biomedical applications," Discover Nano, vol. 18, no. 153, Dec. 2023, doi: 10.1186/s11671-023-03938-x.

[40] Fan, X., Wang, B., Khokhar, M. Q., Zahid, M. A., Pham, D. P., & Yi, J. (2023). Real-Time ITO Layer Thickness for Solar Cells Using Deep Learning and Optical Interference Phenomena. Energies, 16(16), 6049. https://doi.org/10.3390/en16166049

[41] Mitzi, D. B., Gunawan, O., Todorov, T. K., Wang, K., & Guha, S. (2017). Copper indium gallium selenide based solar cells – Review. Energy & Environmental Science, 9(11), 3472–3491. https://doi.org/10.1039/C7EE00826K

[42] C. H. Park, J. Y. Kim, S.-J. Sung, and D.-H. Kim, "Design of grating Al2O3 passivation structure optimized for high-efficiency Cu(In,Ga)Se2 solar cells," *Sensors*, vol. 21, no. 14, Art. no. 4849, Jul. 2021, doi: 10.3390/s21144849.